J. Synchrotron Rad. (1998). **5**, 48–53

A New Apparatus for Polarized X-ray Absorption Fine Structure Using Grazing-Incidence Fluorescence Excitation

Hiroyuki Oyanagi

Electrotechnical Laboratory, Umezono, Tsukuba, Ibaraki 305, Japan.
E-mail: oyanagi@etl.go.jp

(*Received 10 June 1997; accepted 20 August 1997*)

A new apparatus is described for surface-sensitive X-ray absorption fine structure (XAFS) at the 27-pole wiggler beamline BL13B at the Photon Factory. The apparatus is designed for polarized XAFS experiments at low temperature. A closed-cycle helium cryostat is rotated around the ω axis of a vertically mounted high-precision goniometer. The apparatus can be used for XAFS and X-ray standing-wave experiments, sharing a 19-element pure-Ge detector array as a fluorescence detector. The available temperature range is 15–300 K. The performance is demonstrated by in-plane polarized Cu *K*-EXAFS for a $YBa_2Cu_3O_7$ thin film ($\sim$1000 Å) epitaxically grown on an $SrTiO_3$ single crystal. An *in-situ* study of amorphous selenium under optical excitation revealed that neutral defect pairs (C_0^3–C_0^3) are formed by photoexcitation of lone pairs. This indicates that grazing-incidence fluorescence excitation is advantageous for 'pump-and-probe' experiments which can minimize the mismatch in the probing depth between X-ray and optical excitation.

Keywords: XAFS; X-ray standing waves; grazing incidence; fluorescence excitation; pump-and-probe spectroscopy.

1. Introduction

X-ray absorption fine structure (XAFS) is a powerful probe of local structure. For dilute systems a fluorescence detection technique (Jaklevic *et al.*, 1977) is widely used. For surface studies, where a typical density of adsorbed atoms is of the order of 10^{14} cm^{-2}, a grazing-incidence geometry (Becker, Golvchenko & Patel, 1983; Heald, Keller & Stern, 1984) can provide a means of surface-sensitive measurement. Owing to the recent advances of synchrotron radiation, *i.e.* insertion devices such as wigglers and undulators, and a densely packed solid-state detector array, rapid and sensitive measurements of surface XAFS have been achieved (Oyanagi, Shioda, Kuwahara & Haga, 1995).

Recently, temperature-dependent polarized XAFS in fluorescence mode has been applied to studies of spatial modulations in the CuO_2 plane of high critical temperature (T_c) superconductors (Bianconi, Saini, Lanzara *et al.*, 1996; Bianconi, Saini, Rossetti *et al.*, 1996; Bianconi, Lusignoli *et al.*, 1996). Bianconi *et al.* found the mesoscopic scale charge stripe at low temperature using fluorescence XAFS on bulk single crystals. On the other hand, for oxide layers epitaxically grown on single-crystal substrates, grazing-incidence fluorescence excitation was used to minimize the scattering from substrate materials (Oyanagi, Kimura, Terashima & Bando, 1995). These experiments require precise sample orientation at low temperature. For excited-state spectroscopy under illumination, or 'pump-and-probe' spectroscopy (Kolobov, Oyanagi, Tanaka & Tanaka, 1997), a grazing-incidence geometry is important from another viewpoint, *i.e.* it can match the X-ray probe depth with that of optical excitation. For both applications, however, the incidence angle (typically 1° or less) must be precisely controlled, keeping the sample at low temperature. Taking this fact into account it became clear that a new XAFS 'goniometer' should be developed which allows a sample within a cryostat to be oriented with a high resolution (0.002°) and precision (0.1°) in angle.

In order to meet these demands a new apparatus has been designed and built. In the present system a high-precision commercial goniometer (Huber 420) is used to rotate a closed-cycle helium cryostat around the ω axis. This allows one to measure polarized XAFS, including a grazing-incidence geometry, for both parallel and perpendicular sample orientations with respect to the electrical field vector, ε. Moreover, the rear beam monitor can be rotated around the ω axis so that the X-ray standing-wave (XSW) experiment can be performed sharing the experimental set-up. This is an important feature for the surface studies for which XAFS and XSW experiments are complementary and both experiments are desirable. In this paper the design, specifications and performance of a new XAFS apparatus are described.

2. Experimental set-up

2.1. *Geometry*

The basic geometry for XAFS experiments in transmission mode and fluorescence mode are illustrated in Figs.

1(*a*) and 1(*b*), respectively. In this geometry the cold-head axis coincides with the ω axis of a vertically mounted Huber 420 goniometer. The latter geometry (*b*) is also used for a grazing-incidence set-up with the electrical field vector, ε, almost perpendicular to the surface plane (*ab* plane). For monitoring fluorescence the bottom of a cryostat shroud is used as an X-ray window. A Kapton window (100 μm) is directly glued to the shroud.

In Fig. 1(*c*) the geometry for grazing-incidence fluorescence excitation with ε parallel to the *ab* plane is illustrated. In this geometry the rotation of the ω axis changes the grazing-incidence angle but the in-plane polarization is kept constant. For epitaxically grown thin films on single-crystal substrates one can measure XAFS spectra with an optimized probing depth by choosing the proper incidence angle. In this experiment an incidence angle of 1.6° was used. Using either the (*b*) or (*c*) configuration, temperature-dependent XAFS with in-plane ($\varepsilon//ab$) or out-of-plane ($\varepsilon//c$) polarization is easily obtained.

For other experiments the standard aluminium sample holder and shroud can be replaced by special cells, such as a high-temperature furnace, a gas cell or an electrochemistry cell. Fig. 2 shows a small electrochemistry cell mounted horizontally on the ω axis. XAFS (Abruna, 1991) and X-ray diffraction (Zegenhagen *et al.*, 1996) have been successfully used for structural studies of electrochemistry (Kondo, Tamura, Koinuma, Oyanagi & Uosaki, 1997). The advantage of the present arrangement is that both XSW and XAFS experiments can be performed using the same set-up. For copper nanoclusters electrochemically deposited on *p*-type GaAs (001) it was demonstrated that the nanoclusters initially develop in the form of dimers with a coverage, θ,

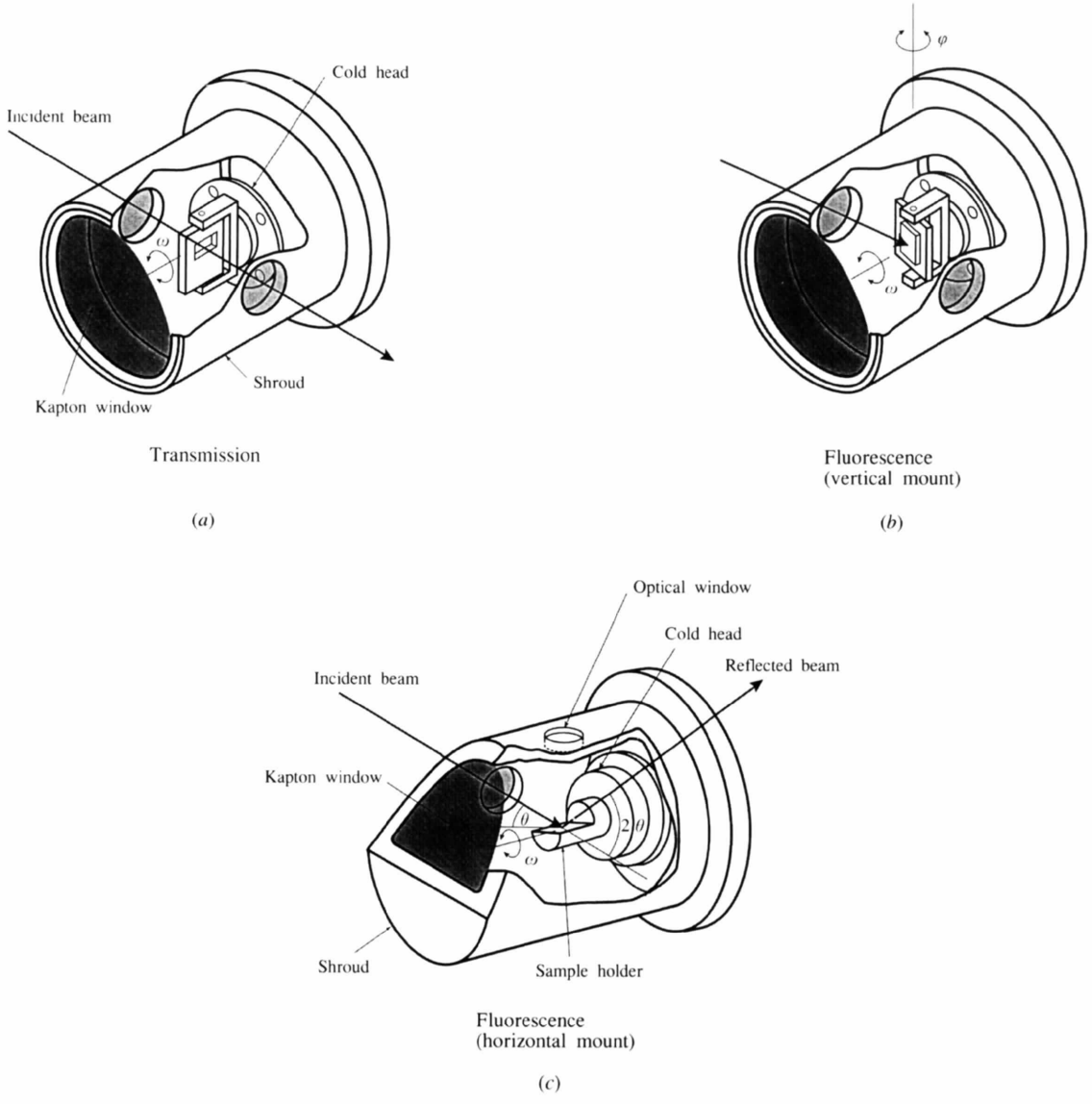

Figure 1
Arrangements of the sample in (*a*) transmission mode and (*b*) fluorescence mode. The two arrangements are easily chosen using a two-axis sample holder attached to the cold finger of a cryostat. The shaded region indicates the Kapton windows. (*c*) Grazing-incidence geometry for surface-sensitive fluorescence detection. A large solid angle is achieved by a tilted Kapton window (shaded area). An optical (Mylar) window is used for photoexcitation of the sample (see text).

below 1 monolayer (ML), while three-dimensional growth is observed for thicker layers (θ > 1 ML). In Fig. 2 the arrangement of detectors, *i.e.* a 19-element solid-state detector array and two ion chambers (I_0 and I), and a sample (electrochemistry cell) are shown in the top photograph. An enlargement of the electrochemistry cell mounted on the cold head is shown in the bottom photograph.

2.2. *Goniometer*

The Huber 420 goniometer is used for rotating the cryostat around the ω axis. Around the same axis the high-precision rotary table is attached for 2θ rotation of the rear ion chamber. The rear ion chamber is used as a monitor of transmitted and reflected beam intensity (the latter for a total reflection regime) in XAFS experiments or reflected beam intensity in XSW experiments. In Fig. 3 the experimental set-up is schematically illustrated. For ω-axis rotation the minimum step angle is 0.0004° and the permitted angle range is ±180°. The cryostat is inserted into the centre borehole of the Huber 420 goniometer of diameter 190 mm. For the Huber 420 goniometer the absolute angle deviation is 20 arcsec and the positioning reproducibility is 2 arcsec. A high resolution in the ω axis is required in experiments in a total reflection regime, where the grazing-incidence angle is of the order of milliradians.

For fine adjustment of the beam position the goniometer is mounted on an XZ stage which is driven by five-phase stepping motors. The translational stroke for X motion (perpendicular to the incident beam) is ±20 mm while that for Z motion (vertical) is ±10 mm. The goniometer can also be rotated around the φ axis on the baseplate (XZ stage) which allows the vertically mounted sample surface to be tilted so that grazing-incidence geometry is achieved. The maximum range in angle for the φ-axis tilt is ±3°. The ω-axis, X, Z and φ-axis motions are controlled by a manual stepping-motor controller (Tsuji Electric Company, PM3C01). In front of the goniometer an XY slit, ionization chamber (length of electrode: 140 mm) and a channel-cut crystal monochromator for XSW experiments are installed. For a rear beam monitor an ionization chamber (length of electrode: 280 mm) is used.

A 27-pole wiggler with a maximum magnetic field, B_0, of 1.5 T inserted into a straight section of the 2.5 GeV storage ring at the Photon Factory was used. The calculated total power of the wiggler was 5.44 kW at B_0 = 1.5 T, with which a brilliance greater than that of a bending magnet by more than an order of magnitude can be obtained over a wide energy range (4–30 keV). White X-rays were monochromated by a fixed-exit double-crystal monochromator (Oyanagi, Haga & Kuwahara, 1996) which horizontally focuses the output beam by sagittal bending of the second crystal.

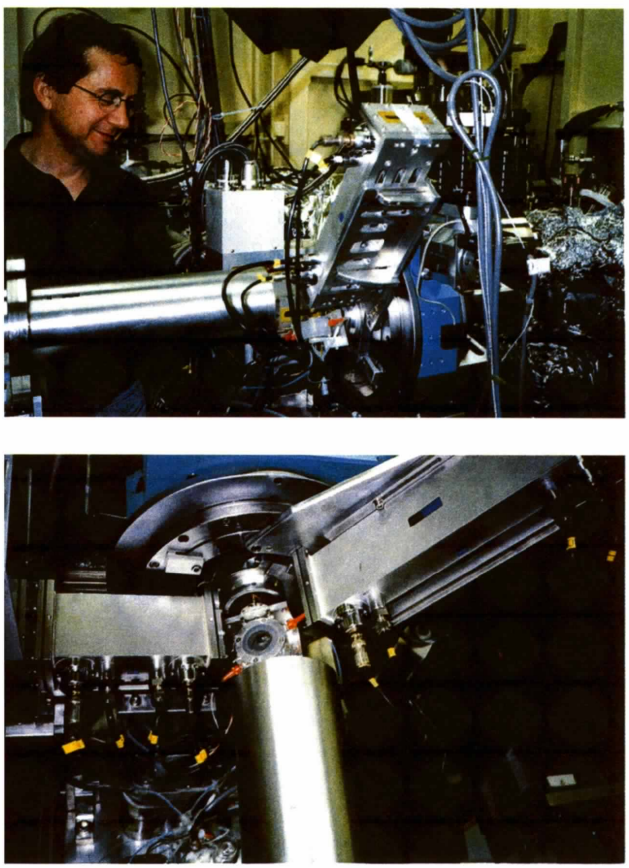

Figure 2
Photograph of the experimental set-up for XSW (top). A small electrochemistry cell is attached to the cryostat (bottom).

2.3. *Fluorescence detector*

The detector array was designed for operation in the 4–30 keV energy range as a fluorescence detector (Oyanagi, Martini & Saito, 1997). The outer diameter of the endcap is 110 mm. Each detector element is made with an n-type high-purity Ge crystal of diameter 11.3 mm and depth 10 mm. The energy rate is greater than 750 MeV s^{-1}. In this arrangement all elements are densely packed with a centre-to-centre spacing of 14.0 mm. The packing ratio of the present detector array is 57%, which is a significant improvement over that of the standard 13-element array (37%) (Cramer, Tench, Yocum & George, 1988). A pure Ge element is mounted with a light-emitting diode and a first field-emitting transistor of the pulsed optical feedback preamplifier in an aluminium capsule.

The detector array is mounted on a motor-controlled XZ stage and its position (height and sample-to-detector distance) can be adjusted. The detector can also be tilted up to 20° on the XZ stage. These adjustments are important to optimize the detector solid angle. After a dead-time correction a linear response with a count rate of 2×10^5 counts s^{-1} was obtained. The total maximum count rate is thus evaluated to be $\sim 3.8 \times 10^6$ counts s^{-1}. The energy resolution was determined for each channel from the full width at half maximum of an Mn $K\alpha$ peak (5.9 keV) using a standard source (^{55}Fe). The average energy resolution over

19 channels is 173 eV at a low count rate using a shaping time constant of 6 μs.

3. Performance

3.1. *Temperature dependence of polarized XAFS*

Fig. 4 compares the Cu $K\alpha$ fluorescence yield spectra for 1000 Å-thick $YBa_2Cu_3O_7$ deposited on an $SrTiO_3$ substrate with the two different geometries, *i.e.* vertical (Fig. 1*b*) and horizontal (Fig. 1*c*). Rotating the entire apparatus around the φ axis, the in-plane polarization data were measured using the vertical geometry, while the ω axis was used to achieve grazing-incidence fluorescence excitation in the horizontal geometry (see Fig. 3). The incidence angle was chosen to be ~1.6°. Measurements were carried out for the former geometry at 57.5 ± 0.1 K and for the latter at 59 ± 0.1 K. A 6 μm Ni filter was inserted between the detector and the sample to reduce the elastic scattering. Below the absorption edge only the fluorescence lines (Ti $K\alpha,\beta$) from the $SrTiO_3$ substrate are observed. The data were obtained by a single scan integrating the fluorescence signal for 5 s per data point, averaging data from 15 out of 19 channels. One can see that there are glitches at ~9.5 keV in the data taken with the vertical geometry. These glitches, due to strong diffraction from the $SrTiO_3$ substrate, are absent in the data taken in the horizontal geometry.

In Fig. 5 the normalized Cu *K*-EXAFS oscillations are shown for the two data sets in Fig. 4. One can see that the glitches at $k \simeq 12$ Å^{-1} strongly distort the spectrum, and small features in the high-k region, *i.e.* ~14 Å^{-1}, are missing in the vertical geometry. The results show that high-quality in-plane polarized EXAFS data can be obtained for a thin epilayer grown on a single-crystal substrate if horizontal grazing-incidence fluorescence excitation is used. A large anisotropy observed in the near-edge and EXAFS oscillations with respect to the polarization vector was in agreement with the crystal structure and previous reports.

It was found that the local structure in the CuO_2 plane becomes distorted at low temperature, indicating the existence of the two domains with different Cu—O bond lengths, *i.e.* on decreasing temperature below T_c the second domain associated with an elongated Cu—O bond increased its population. Details of temperature-dependent local lattice anomalies are reported elsewhere (Oyanagi & Zegenhagen, 1997). In a recently proposed model (Bianconi, Saini, Lanzara *et al.*, 1996; Bianconi, Saini, Rossetti *et al.*, 1996; Bianconi, Lusignoli *et al.*, 1996) the two components, *i.e.* locally distorted (localized) and undistorted (itinerant) domains, form the two-dimensional superlattice which might enhance T_c as a quantum effect. The observed two-domain structure in $YBa_2Cu_3O_7$ at low temperature is consistent with a stripe model. If the two-dimensional stripe in 123 compounds is confirmed by the superstructure, the spatial modulations in the CuO_2 plane will be generalized and the role of lattice anomalies in high-T_c superconductivity will be clear.

3.2. *Pump-and-probe XAFS*

Photostructural change in amorphous selenium (a-Se) has been studied *in situ* by extended X-ray absorption fine structure (EXAFS) at 30 K (Kolobov *et al.*, 1997). The sample was mounted on an aluminium holder in an

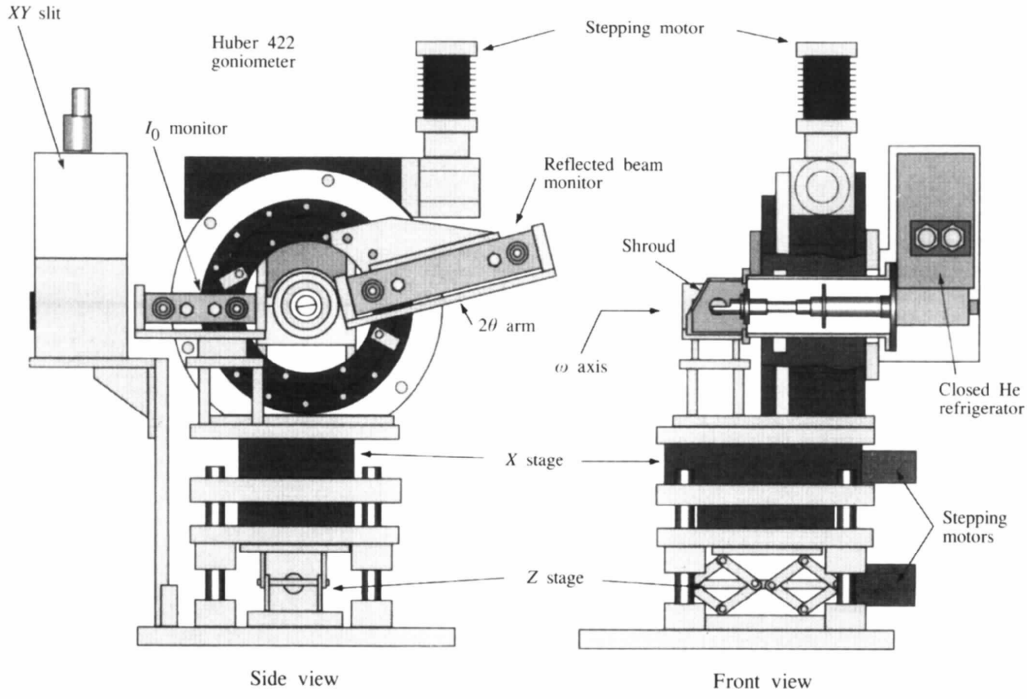

Figure 3
Experimental set-up around the goniometer and a detector. The Huber 420 goniometer is vertically mounted. A 19-element pure-Ge detector array is used for fluorescence detection.

evacuated cryostat equipped with windows (Kapton) for incident and fluorescent X-ray beams as well as an optical window (Mylar) for *in-situ* light irradiation. In Fig. 1(*c*) the optical window is indicated in the top portion of the shroud. A 500 W Xe lamp with an IR cut-off filter was used as an excitation source. The light was focused onto a 15 mm diameter spot for which the light intensity on the surface of the sample varied from 50 to 250 mW cm^{-2}. A closed-cycle

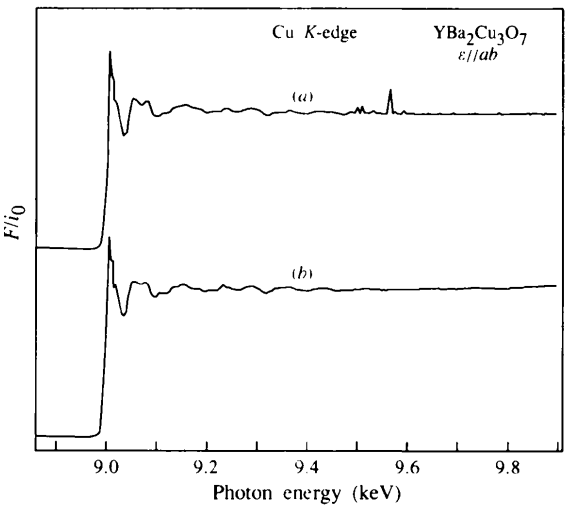

Figure 4
Cu $K\alpha$ fluorescence yield spectra for $YBa_2Cu_3O_7$ (1000 Å) on an $SrTiO_3$ single-crystal taken with ε parallel to the *ab* plane using the grazing-incidence geometry (*a*) (top) and (*b*) (bottom).

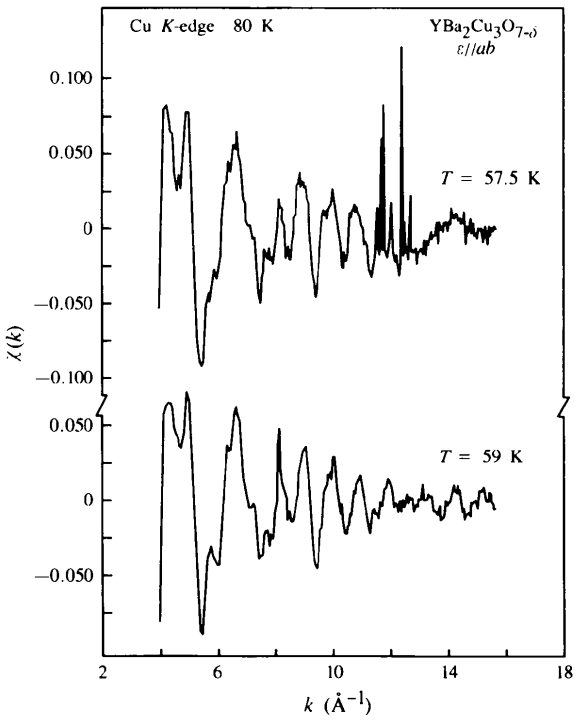

Figure 5
Normalized Cu *K*-EXAFS oscillations for $YBa_2Cu_3O_7$ (1000 Å) as a function of photoelectron wave number ($Å^{-1}$) taken from the data shown in Fig. 4.

He refrigerator with a cooling power of ~9 W at 20 K was used.

Fig. 6 shows normalized Se *K*-EXAFS oscillations for a-Se where solid and dashed lines indicate the data taken prior to and under illumination, respectively. The lower curve indicates the data for crystalline Se. All data were measured in fluorescence mode at 30 K. One can see that under illumination at low temperature the magnitude of EXAFS oscillations for a-Se increases slightly. By carefully analyzing the first nearest neighbour contribution and the correlation among the structural parameters it was found that the coordination of Se atoms is modified by photoexcitation. We observed an increase in the average coordination number by ~4% and mean-square relative displacement while the Se—Se bond length is essentially unchanged. These changes can be attributed to the local formation of threefold-coordinated defect sites, which simultaneously increase the structural disorder or the mean-square relative displacements, σ^2.

The essential feature of the observed photoinduced change of the coordination is *dynamical*, *i.e.* the initial twofold coordination is restored immediately after switching off the light, while the increased structural disorder partly remains. Details of the experimental set-up for photo-excited-state spectroscopy are described elsewhere (Kolobov *et al.*, 1997). The results demonstrate the capability of grazing-incidence XAFS as a means of direct measurement

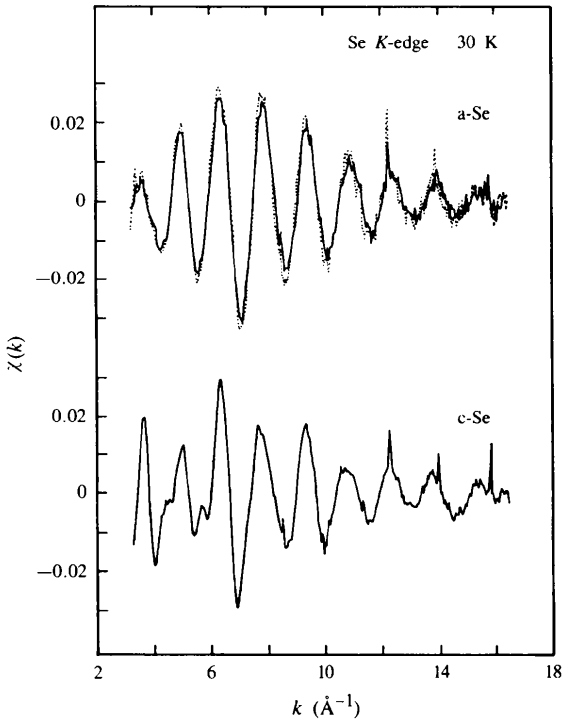

Figure 6
The upper curves indicate normalized Se *K*-EXAFS oscillations for amorphous Se (a-Se) where solid and dashed lines indicate the data taken prior to and under illumination, respectively. The lower curve indicates the data for crystalline Se (c-Se). All data were measured in fluorescence mode at 30 K.

of the local structure during photoexcitation. For *in-situ* 'pump-and-probe' experiments the use of grazing-incidence fluorescence excitation is essential for probing the optically excited regions in a hard X-ray region. The use of a horizontal geometry is convenient for matching the optical and X-ray probing depths since one can avoid the use of thick films which are difficult to optically excite the material effectively.

4. Summary

We have reported a versatile apparatus for polarized fluorescence XAFS equipped with a vertically mounted high-precision goniometer with a closed-cycle helium cryostat. This arrangement allows one to measure polarized fluorescence XAFS at low temperature. For vertical and horizontal sample orientations grazing-incidence fluorescence excitation is achieved using the ω axis of the goniometer and the φ axis of the baseplate, respectively. The apparatus is also capable of XSW experiments using the same experimental set-up. Grazing-incidence fluorescence excitation is particularly advantageous for epitaxic thin films. Application to a $YBa_2Cu_3O_7$ epitaxic layer grown on an $SrTiO_3$ substrate demonstrates that high-quality data are obtained for in-plane ($\varepsilon//ab$) and out-of-plane ($\varepsilon//c$) polarizations. Another advantage of grazing-incidence fluorescence excitation is that the probing depth can match with that of optical excitation. Application to photostructural change in amorphous selenium showed that this technique can be a promising means of 'pump-and-probe' X-ray spectroscopy.

The author expresses his greatest thanks to A. Kolobov, T. Kondo, K. Tamura, K. Uosaki, J. Zegenhagen, N. L. Saini and S. Wei for helpful suggestions and technical assistance. $YBa_2Cu_3O_7$ samples were kindly supplied by A. Sawa and M. Koyanagi. The author also wishes to thank A. Bianconi, H. Simizu and K. Tanaka for warm encouragement. This work has been performed as part of a collaborative project between the Electrotechnical Laboratory and the Photon Factory, National Institute for High Energy Physics (KEK).

References

Abruna, H. (1991). Editor. *Electrochemical Interfaces: Modern Techniques for In-Situ Interface Characterization*. New York: VCH.

Becker, R. S., Golvchenko, J. A. & Patel, J. R. (1983). *Phys. Rev. Lett.* **50**, 153–156.

Bianconi, A., Lusignoli, M., Saini, N. L., Bordet, P., Kvick, Å. & Radaelli, P. G. (1996). *Phys. Rev. B*, **54**, 4310–4314.

Bianconi, A., Saini, N. L., Lanzara, A., Missori, M., Rossetti, T., Oyanagi, H., Yamaguchi, H., Oka, K. & Ito, T. (1996). *Phys. Rev. Lett.* **76**, 3412–3415.

Bianconi, A., Saini, N. L., Rossetti, T., Lanzara, A., Perali, A., Missori, M., Oyanagi, H., Yamaguchi, H. & Nishihara, Y. (1996). *Phys. Rev. B*, **54**, 12018–12021.

Cramer, S. P., Tench, O., Yocum, M. & George, G. N. (1988). *Nucl. Instrum. Methods*, A**266**, 586–591.

Heald, S. M., Keller, E. & Stern, E. A. (1984). *Phys. Lett.* A**103**, 155–158.

Jaklevic, J., Kirby, J. A., Klein, M. P., Robertson, A. S., Brown, G. S. & Eisenberger, P. (1977). *Solid State Commun.* **23**, 679–682.

Kolobov, A., Oyanagi, H., Tanaka, K. & Tanaka, Ke. (1997). *Phys. Rev. B*, **55**, 726–734.

Kondo, T., Tamura, K., Koinuma, M., Oyanagi, H. & Uosaki, K. (1997). *Chem. Lett.* pp. 761–762.

Oyanagi, H., Haga, K. & Kuwahara, K. (1996). *Rev. Sci. Instrum.* **67**, 350–354.

Oyanagi, H., Kimura, H., Terashima, T. & Bando, Y. (1995). *J. Phys. Soc. Jpn*, **64**, 2563–2571.

Oyanagi, H., Martini, M. & Saito, M. (1997). *Nucl. Instrum. Methods*. In the press.

Oyanagi, H., Shioda, R., Kuwahara, Y. & Haga, K. (1995). *J. Synchrotron Rad.* **2**, 99–105.

Oyanagi, H. & Zegenhagen, J. (1997). *J. Supercond.* **10**, 415–419.

Zegenhagen, J., Kazimirov, A., Scherb, G., Kolb, D. M., Smilgies, D.-M. & Feidenhans'l, R. (1996). *Surf. Sci.* **352/354**, 346–351.